

# Role of octupole shape degree of freedom in neutron-rich odd-mass xenon isotopes

K. Nomura\*

*Department of Physics, Hokkaido University, Sapporo 060-0810, Japan and  
Nuclear Reaction Data Center, Hokkaido University, Sapporo 060-0810, Japan*

(Dated: December 5, 2024)

Influences of the octupole shape degree of freedom on low-energy spectra of neutron-rich odd-mass xenon isotopes are studied within the interacting boson-fermion model that is based on the nuclear density functional theory. The interacting-boson Hamiltonian describing low-energy quadrupole and octupole collective states of the even-even nuclei  $^{140,142,144}\text{Xe}$ , single-particle energies, and occupation probabilities for an unpaired neutron in the odd-mass nuclei  $^{141,143,145}\text{Xe}$ , are determined based on the axially symmetric quadrupole-octupole deformation-constrained self-consistent mean-field calculations with a choice of the energy density functional and pairing interaction. Strength parameters of the boson-fermion interactions are empirically determined to reproduce a few low-lying levels of each odd-mass nucleus. The mean-field calculation predicts for  $^{142}\text{Xe}$  a potential energy surface that is notably soft in the octupole deformation with a non-zero octupole global minimum. The octupole correlations are shown to be relevant in positive-parity excited states of  $^{143,145}\text{Xe}$ .

## I. INTRODUCTION

Search for the reflection asymmetric, octupole deformation in nuclei has been a recurrent theme of interest that is under active investigations for several decades. The octupole correlations are considered to be enhanced in several specific mass regions corresponding to the neutron  $N$  and/or proton  $Z$  numbers equal to 34, 56, 88, 134, ..., in which coupling between the normal and unique-parity single-particle orbitals differing in the total and orbital angular momenta by  $3\hbar$  is possible [1]. Most of those nuclei with the aforementioned nucleon numbers are short lived, but have recently become accessible by experiments using radioactive beams. In addition, since observation of a large electric dipole moment in the octupole-deformed nucleus would indicate violation of time-reversal (T) or charge-parity (CP) symmetry, it is also relevant to a possible extension of the standard model of particle physics [2]. Evidence for a static octupole deformation was found in light actinide region, i.e.,  $^{220}\text{Rn}$  and  $^{224}\text{Ra}$ , by the experiment at ISOLDE, CERN [3]. The experiments carried out at Argonne National Laboratory found another candidates for the octupole deformation in the neutron-rich region, i.e.,  $^{144}\text{Ba}$  [4] and  $^{146}\text{Ba}$  [5].

The present study is focused on the octupole correlation effects in the neutron-rich even- and odd-mass Xe isotopes in the “north east” of the doubly magic nucleus  $^{132}\text{Sn}$ . Since in this mass region octupole collectivity is supposed to be most pronounced in the neighborhood of the  $^{144}\text{Ba}$  nucleus (with  $N = 88$  and  $Z = 56$ ), it is of interest to see if the octupole degree of freedom still plays a role in the Xe isotopes with  $N \approx 88$ . Spectroscopic data for the neutron-rich Xe isotopes are also available. For example, in the  $\beta$ -decay study performed as part of the EURICA project in RIKEN, level structure of the

neutron-rich  $^{140}\text{Xe}$  nucleus was determined [6], and this study has been extended further to those of the odd-mass nuclei  $^{141,143}\text{Xe}$  [7, 8]. The fact that new data both on the even-even and odd-even neutron-rich Xe isotopes have become available thus necessitates theoretical investigations in a timely manner, that allow for a systematic as well as quantitative prediction on the details of their low-lying structures.

The theoretical method employed in the present study is the interacting boson model (IBM) that is based on the nuclear density functional theory. The starting point is the constrained self-consistent mean-field (SCMF) calculations with a choice of the energy density functional (EDF) and pairing interaction, providing the potential energy surface (PES) as a function of the axially symmetric quadrupole and octupole deformations. The quadrupole-octupole SCMF PES is then mapped onto the expectation value of the Hamiltonian of the IBM, that consists of monopole  $s$  (with spin and parity  $J^\pi = 0^+$ ), quadrupole  $d$  ( $J^\pi = 2^+$ ), and octupole  $f$  ( $J^\pi = 3^-$ ) bosons. The mapping procedure specifies the  $sdf$ -IBM Hamiltonian describing low-lying positive- and negative-parity states of even-even nuclei. Odd-mass nuclei are dealt with by means of the particle-boson coupling in the interacting boson-fermion model (IBFM) [9], with the even-even  $sdf$ -IBM core Hamiltonian determined by the mapping procedure. The same SCMF calculations provide microscopic input to determine most parts of the  $sdf$ -IBFM Hamiltonian. Strength parameters for the boson-fermion interactions are, however, obtained empirically to reproduce low-energy spectra of each odd-mass nucleus.

The mapped  $sdf$ -IBM has been extensively used to study low-energy quadrupole and octupole collective states for those even-even nuclei in light actinide [10–12], rare-earth [11], lanthanide [11, 13], neutron-rich  $A \approx 100$  [14], and neutron-deficient  $N \approx Z \approx 34$  [15] regions. In Ref. [16], in particular, the  $sdf$ -IBFM framework has been developed and applied to the neutron-rich odd-mass

\* nomura@sci.hokudai.ac.jp

$^{143,145,147}\text{Ba}$  nuclei with the microscopic input obtained from the relativistic EDF. The *sdf*-IBFM produced for  $^{143,145,147}\text{Ba}$  low-energy band structures in agreement with data [17, 18], and suggested some excited bands that can be interpreted as octupole bands connected by the *E3* transitions to ground-state bands. Earlier experiments on the  $^{141,143}\text{Xe}$  nuclei [19–21] suggested more or less similar low-lying band structures to those observed for the neighboring  $^{143,145}\text{Ba}$  nuclei. It is thus feasible to extend the *sdf*-IBFM calculation to the Xe isotopes, since similar model parameters to those used for the odd-mass Ba could be employed.

In Sec. II the theoretical procedure is described. Results of the mean-field calculations and spectroscopic calculations within the *sdf*-IBM for the even-even Xe isotopes are discussed in Sec. III. In Sec. IV calculated energy levels and transition properties for the odd-mass Xe nuclei within the *sdf*-IBFM are reported. Summary of the main results and conclusions are given in Sec. V.

## II. THEORETICAL FRAMEWORK

The constrained SCMF calculations are carried out within the relativistic Hartree-Bogoliubov (RHB) model [22, 23] using the density-dependent point-coupling (DD-PC1) [24] functional for particle-hole channel and a separable pairing force of finite range [25] in the particle-particle channel. The constraints are those on the axially symmetric mass quadrupole  $Q_{20}$  and octupole  $Q_{30}$  moments, which are related to the dimensionless shape variables  $\beta_2$  and  $\beta_3$ , respectively:

$$\beta_\lambda = \frac{4\pi}{3AR^\lambda} Q_{\lambda 0} \quad (1)$$

with  $\lambda = 2$  or  $3$ , and  $R = 1.2A^{1/3}$  fm. The RHB-SCMF calculations produce for the even-even  $^{140,142,144}\text{Xe}$  nuclei the  $(\beta_2, \beta_3)$ -PESs, which are used to determine the *sdf*-IBM Hamiltonian by the procedure described below.

The even-even core nuclei are here described in terms of the interacting *s*, *d*, and *f* bosons [26, 27], which are microscopically interpreted as the monopole, quadrupole, and octupole collective pairs of valence nucleons, respectively, as in the *sd*-IBM framework [28–30]. The odd-mass nucleus is described as a coupled system of the even-even IBM core and an unpaired nucleon. The *sdf*-IBFM Hamiltonian is given in general as

$$\hat{H}_{\text{IBFM}} = \hat{H}_{\text{B}} + \hat{H}_{\text{F}} + \hat{V}_{\text{BF}} , \quad (2)$$

where the first, second, and third terms on the right-hand side represent the *sdf*-IBM Hamiltonian, single-fermion Hamiltonian, and boson-fermion interaction, respectively. Here  $\hat{H}_{\text{B}}$  takes the form

$$\hat{H}_{\text{B}} = \epsilon_d \hat{n}_d + \epsilon_f \hat{n}_f + \kappa_2 \hat{Q} \cdot \hat{Q} + \kappa_3 \hat{O} \cdot \hat{O} + \kappa' \hat{L} \cdot \hat{L} . \quad (3)$$

In the first (second) term,  $\hat{n}_d = d^\dagger \cdot \tilde{d}$  ( $\hat{n}_f = f^\dagger \cdot \tilde{f}$ ), with  $\epsilon_d$  ( $\epsilon_f$ ) representing the single *d* (*f*) boson energy

relative to the *s*-boson one. Note  $\tilde{d}_\mu = (-1)^\mu d_{-\mu}$  and  $\tilde{f}_\mu = (-1)^{3+\mu} f_{-\mu}$ . The third and fourth terms in (3) stand for quadrupole-quadrupole and octupole-octupole interactions, respectively. The quadrupole  $\hat{Q}$  and octupole  $\hat{O}$  operators read

$$\hat{Q} = s^\dagger \tilde{d} + d^\dagger s + \chi (d^\dagger \times \tilde{d})^{(2)} + \chi' (f^\dagger \times \tilde{f})^{(2)} , \quad (4)$$

$$\hat{O} = s^\dagger \tilde{f} + f^\dagger s + \chi'' (d^\dagger \times \tilde{f} + f^\dagger \times \tilde{d})^{(3)} , \quad (5)$$

with  $\chi$ ,  $\chi'$ , and  $\chi''$  being dimensionless parameters. The last term in Eq. (3),  $\hat{L} \cdot \hat{L}$ , is introduced to better describe moments of inertia of yrast bands, with  $\hat{L}$  being the boson angular momentum operator

$$\hat{L} = \sqrt{10}(d^\dagger \times \tilde{d})^{(1)} - \sqrt{28}(f^\dagger \times \tilde{f})^{(1)} . \quad (6)$$

The form of the *sdf*-IBM Hamiltonian in Eq. (3) is slightly different from that employed in the previous study on odd-mass Ba [16]: in Ref. [16] the octupole-octupole term was taken to be of the form,  $:\hat{V}_3^\dagger \cdot \hat{V}_3:$ , where  $\hat{V}_3^\dagger = s^\dagger \tilde{f} + \chi''(d^\dagger \times \tilde{f})^{(3)}$  and the notation  $:(\ ):$  represents normal ordering, and the angular momentum operator in the  $\hat{L} \cdot \hat{L}$  term consisted only of the *d*-boson term, i.e.,  $\hat{L} = \sqrt{10}(d^\dagger \times \tilde{d})^{(1)}$ .

The boson analog of the  $(\beta_2, \beta_3)$ -PES is given by the energy expectation value  $E_{\text{IBM}}(\beta_2, \beta_3) = \langle \phi(\beta_2, \beta_3) | \hat{H}_{\text{B}} | \phi(\beta_2, \beta_3) \rangle$ . Here  $|\phi(\beta_2, \beta_3)\rangle$  represents the coherent state [31] of *s*, *d*, and *f* bosons, given by

$$|\phi(\beta_2, \beta_3)\rangle = (s^\dagger + \bar{\beta}_2 d_0^\dagger + \bar{\beta}_3 f_0^\dagger)^n |0\rangle , \quad (7)$$

up to a normalization factor, where  $n$  is the number of bosons, i.e., valence nucleon pairs,  $\bar{\beta}_\lambda$  is a boson analog of the quadrupole ( $\lambda = 2$ ) or octupole ( $\lambda = 3$ ) deformation variable in the geometrical model [32], and  $|0\rangle$  represents the inert core, or the doubly-magic nucleus  $^{132}\text{Sn}$ . It is assumed that bosonic deformation is proportional to the geometrical one, that is,  $\bar{\beta}_\lambda = C_\lambda \beta_\lambda$ , where  $C_\lambda$  stands for a constant of proportionality.

The *sdf*-IBM Hamiltonian (3) is determined for each nucleus by mapping the RHB-SCMF PES,  $E_{\text{SCMF}}(\beta_2, \beta_3)$ , onto the bosonic counterpart,  $E_{\text{IBM}}(\beta_2, \beta_3)$ , so that both energy surfaces become similar in topology in the neighborhood of the global minimum [11, 33, 34],  $E_{\text{SCMF}}(\beta_2, \beta_3) \approx E_{\text{IBM}}(\beta_2, \beta_3)$ . The mapping procedure determines the strength parameters for  $\hat{H}_{\text{B}}$  together with the constants  $C_2$  and  $C_3$ . However, since the  $\hat{L} \cdot \hat{L}$  term does not make a contribution to the PES, its strength parameter  $\kappa'$  has to be determined in a separately way, so that the moment of inertia calculated in the boson intrinsic state [35] at the equilibrium minimum should be equal to the corresponding cranking moment of inertia computed with the RHB-SCMF method using the Inglis-Belyaev (IB) formula [36, 37]. The IB moment of inertia is here increased by 30 % in order to account for the fact the IB formula significantly underestimates the empirical moments of inertia. See Ref. [38] for further details.

Table I lists the parameters for  $\hat{H}_B$  adopted in the present study.

The single-fermion Hamiltonian in Eq. (2) for the odd neutron reads,  $\hat{H}_F = \sum_j \epsilon_j (a_j^\dagger \times \tilde{a}_j)^{(0)}$ , where  $\epsilon_j$  is the single-particle energy,  $a_j^\dagger$  is creation operator for a particle in orbital  $j$ , and  $\tilde{a}_j \equiv (-1)^{j-m} a_{j-m}$  denotes annihilation operator. The fermion valence space for the considered odd-mass nuclei  $^{141,143,145}\text{Xe}$  comprises all single-particle levels in the neutron  $N = 82 - 126$  major oscillator shell, that is,  $3p_{1/2}$ ,  $3p_{3/2}$ ,  $2f_{5/2}$ ,  $2f_{7/2}$ ,  $1h_{9/2}$  and  $1i_{13/2}$ .

The boson-fermion interaction in Eq. (2),  $\hat{V}_{\text{BF}}$ , consists of the terms that represent the coupling of the odd neutron to the  $sd$ -boson space  $\hat{V}_{\text{BF}}^{sd}$ , to the  $f$  boson space  $\hat{V}_{\text{BF}}^f$ , and to the combined  $sd$ -boson space  $\hat{V}_{\text{BF}}^{sd}$ :

$$\hat{V}_{\text{BF}} = \hat{V}_{\text{BF}}^{sd} + \hat{V}_{\text{BF}}^f + \hat{V}_{\text{BF}}^{sd}. \quad (8)$$

The first term in Eq. (8) reads:

$$\begin{aligned} \hat{V}_{\text{BF}}^{sd} = & \sum_{j_a j_b} \Gamma_{j_a j_b}^{sd} \hat{Q}_{sd} \cdot (a_{j_a}^\dagger \times \tilde{a}_{j_b})^{(2)} \\ & + \sum_{j_a j_b j_c} \Lambda_{j_a j_b j_c}^{dd} : \left[ (a_{j_a}^\dagger \times \tilde{d})^{(j_c)} \times (d^\dagger \times \tilde{a}_{j_b})^{(j_c)} \right]^{(0)} \\ & + \sum_{j_a} A_{j_a}^d (a_{j_a}^\dagger \times \tilde{a}_{j_a})^{(0)} \hat{n}_d, \end{aligned} \quad (9)$$

where the first, second and third terms denote quadrupole dynamical, exchange and monopole terms, respectively [9, 39].  $\hat{Q}_{sd}$  is the  $sd$  part of the quadrupole operator in Eq. (4). In this section, single-particle orbitals are denoted by  $j_a, j_b, j_c, \dots$ , while primed ones, such as  $j'_a, j'_b, j'_c, \dots$ , stand for those with opposite parity, unless otherwise specified. In a similar fashion to Eq. (9) the following form is considered for the  $f$ -boson part:

$$\begin{aligned} \hat{V}_{\text{BF}}^f = & \sum_{j_a j_b} \Gamma_{j_a j_b}^{ff} \hat{Q}_{ff} \cdot (a_{j_a}^\dagger \times \tilde{a}_{j_b})^{(2)} \\ & + \sum_{j_a j_b j'_c} \Lambda_{j_a j_b j'_c}^{ff} : \left[ (a_{j_a}^\dagger \times \tilde{f})^{(j'_c)} \times (f^\dagger \times \tilde{a}_{j_b})^{(j'_c)} \right]^{(0)} \\ & + \sum_{j_a} A_{j_a}^f (a_{j_a}^\dagger \times \tilde{a}_{j_a})^{(0)} \hat{n}_f, \end{aligned} \quad (10)$$

TABLE I. The parameters of the  $sd$ -IBM Hamiltonian.  $\epsilon_d$ ,  $\epsilon_f$ ,  $\kappa_2$ ,  $\kappa'$  and  $\kappa_3$  are in units of MeV, and the others are dimensionless.

	$\epsilon_d$	$\epsilon_f$	$\kappa_2$	$\chi$	$\chi'$	$\kappa'$	$\kappa_3$	$\chi''$
$^{140}\text{Xe}$	0.881	0.852	-0.098	-1.2	-1.7	-0.023	0.030	-0.8
$^{142}\text{Xe}$	0.644	0.710	-0.098	-1.3	-2.2	-0.016	0.048	-1.6
$^{144}\text{Xe}$	0.661	0.951	-0.098	-1.3	-2.0	-0.018	0.048	-1.6

where  $\hat{Q}_{ff} = \chi' (f^\dagger \times \tilde{f})^{(2)}$  is identified as the fourth term of the quadrupole operator  $\hat{Q}$  [Eq. (4)]. Finally,  $\hat{V}_{\text{BF}}^{sd}$  in Eq. (8) reads:

$$\begin{aligned} \hat{V}_{\text{BF}}^{sd} = & \sum_{j_a j'_b} \Gamma_{j_a j'_b}^{sd} \hat{O} \cdot [a_{j_a}^\dagger \times \tilde{a}_{j'_b}]^{(3)} \\ & + \sum_{j_a j'_b j_c} \Lambda_{j_a j'_b j_c}^{df} : \left[ [a_{j_a}^\dagger \times \tilde{d}]^{(j_c)} \times [f^\dagger \times \tilde{a}_{j'_b}]^{(j_c)} \right]^{(0)} \\ & + (\text{H.c.}), \end{aligned} \quad (11)$$

where the first and second terms denote the dynamical octupole and exchange terms, respectively.

By using the generalized seniority scheme [39], the  $j$ -dependent coefficients of the three terms in  $\hat{V}_{\text{BF}}^{sd}$  in Eq. (9) are shown to have the forms

$$A_j^d = -A_0^d \sqrt{2j+1} \quad (12)$$

$$\Gamma_{j_a j_b}^{sd} = \Gamma_0^{sd} \gamma_{j_a j_b}^{(2)} \quad (13)$$

$$\Lambda_{j_a j_b j_c}^{dd} = -2\Lambda_0^{dd} \sqrt{\frac{5}{2j_c+1}} \beta_{j_a j_c}^{(2)} \beta_{j_b j_c}^{(2)}, \quad (14)$$

with  $\Gamma_0^{sd}$ ,  $\Lambda_0^{sd}$ ,  $A_0^d$  denoting strength parameters. The above formulas have been extended to  $sd$ -boson systems in Ref. [16], and similar expressions are obtained for the coefficients in  $\hat{V}_{\text{BF}}^f$  and  $\hat{V}_{\text{BF}}^{sd}$ . For the  $f$ -boson part:

$$A_j^f = -A_0^f \sqrt{2j+1} \quad (15)$$

$$\Gamma_{j_a j_b}^{ff} = \Gamma_0^{ff} \gamma_{j_a j_b}^{(2)} \quad (16)$$

$$\Lambda_{j_a j_b j'_c}^{ff} = -2\Lambda_0^{ff} \sqrt{\frac{7}{2j'_c+1}} \beta_{j_a j'_c}^{(3)} \beta_{j_b j'_c}^{(3)} \quad (17)$$

and for the  $sd$ -boson terms:

$$\Gamma_{j_a j'_b}^{sd} = \Gamma_0^{sd} \gamma_{j_a j'_b}^{(3)} \quad (18)$$

$$\Lambda_{j_a j'_b j_c}^{df} = -2\Lambda_0^{df} \sqrt{\frac{7}{2j_c+1}} \beta_{j_a j_c}^{(2)} \beta_{j'_b j_c}^{(3)}. \quad (19)$$

In the expressions in Eqs. (12)–(19)  $\gamma_{ij}^{(\lambda)} = (u_i u_j - v_i v_j) q_{ij}^{(\lambda)}$  and  $\beta_{ij}^{(\lambda)} = (u_i v_j + u_j v_i) q_{ij}^{(\lambda)}$ , where  $v_j$  ( $u_j$ ) is an occupation (unoccupation) amplitude, and  $q_{ij}^{(\lambda)}$  represents the matrix element of fermion quadrupole ( $\lambda = 2$ ) or octupole ( $\lambda = 3$ ) operator in the single-particle basis. Within this framework the single-particle energy  $\epsilon_j$  should be replaced with the quasiparticle energy denoted by  $\tilde{\epsilon}_j$ .  $\tilde{\epsilon}_j$  as well as occupation probabilities  $v_j^2$  for the considered single-particle states are provided by the RHB-SCMF calculations constrained to zero deformation (see Refs. [16, 40] for details). The adopted  $\tilde{\epsilon}_j$  and  $v_j^2$  are listed in Table II.

There are 14 strength parameters for the boson-fermion interaction  $\hat{V}_{\text{BF}}$  that have to be adjusted to the spectroscopic data for the odd-mass Xe isotopes: six ( $\Gamma_0^{sd}$ ,  $\Gamma_0^{ff}$ ,  $\Lambda_0^{dd}$ ,  $\Lambda_0^{ff}$ ,  $A_0^d$  and  $A_0^f$ ) for each of the

normal-parity  $pfh$  (i.e.,  $3p_{1/2,3/2}$ ,  $2f_{5/2,7/2}$ ,  $1h_{9/2}$ ) and the unique-parity  $1i_{13/2}$  single-particle configurations, and two additional parameters  $\Gamma_0^{sd}$  and  $\Lambda_0^{df}$ . Their values are determined by taking the procedure described in the following.

First, the strength parameters  $\Gamma_0^{sd}$ ,  $\Lambda_0^{sd}$ , and  $A_0^d$  for the unique-parity ( $1i_{13/2}$ ) and normal-parity ( $pfh$ ) configurations are determined within the  $sd$ -IBM so as to reproduce, respectively, a few lowest-lying positive- and negative-parity levels for  $^{141,143}\text{Xe}$ . For  $^{143}\text{Xe}$  a  $\Delta I = 2$  band based on the  $I = 9/2$  level without the parity being assigned is experimentally suggested [21], and is here assumed to be a positive-parity band, based on the fact that a  $9/2^+$  band at a similar excitation energy is observed in  $^{145}\text{Ba}$  [17]. The corresponding parameters  $\Gamma_0^{sd}$ ,  $\Lambda_0^{sd}$ , and  $A_0^d$  for the  $1i_{13/2}$  single-particle configuration for  $^{143}\text{Xe}$  are determined so that a few low-lying levels of the parity-unassigned  $I = 9/2$  band are reasonably reproduced. In addition, for the negative-parity states of both  $^{141,143}\text{Xe}$ , a special attention is paid to reproduce the order of the  $5/2_1^-$ ,  $7/2_1^-$ , and  $9/2_1^-$  levels. Note that any energy offset between the lowest negative- and positive-parity states, which is often introduced as a free parameter in the IBFM, is not introduced for all the odd-mass Xe nuclei studied in the present work.

The second step is to determine the parameters  $\Gamma_0^{ff}$ ,  $\Lambda_0^{ff}$ , and  $A_0^f$  within the  $sdf$ -IBFM. For the sake of simplicity, the same values as those used in Ref. [16] are adopted as an initial guess, and are readjusted so that the following conditions should be met for the odd-mass Xe nuclei: (i) the ground state spin should be  $5/2^-$  in the  $sdf$ -IBFM; (ii) for  $^{141}\text{Xe}$ , the  $13/2_1^+$  and  $15/2_1^+$  levels should be close to the measured ones [18]; (iii) for  $^{143}\text{Xe}$ , the calculated  $13/2_1^+$  level should be close to the measured  $13/2$  state at 703 keV [21], and the  $5/2_1^+$  level appears at low energy, since in the  $N = 89$  isotone  $^{145}\text{Ba}$  several  $5/2^+$  levels are observed at the excitation energies  $E_x \approx 0.3 - 0.5$  MeV and a similar structure is expected to occur in  $^{143}\text{Xe}$ . The parameters  $\Gamma_0^{sd}$ ,  $\Lambda_0^{sd}$ , and  $A_0^d$  obtained in the previous step are also slightly modified to accommodate the above conditions.

TABLE II. Quasiparticle energies  $\tilde{\epsilon}_j$  (in MeV) and occupation probabilities  $v_j^2$  of the odd neutron for the orbitals  $3p_{1/2}$ ,  $3p_{3/2}$ ,  $2f_{5/2}$ ,  $2f_{7/2}$ ,  $1h_{9/2}$ , and  $1i_{13/2}$  calculated for  $^{141,143,145}\text{Xe}$  with the RHB-SCMF method.

		$3p_{1/2}$	$3p_{3/2}$	$2f_{5/2}$	$2f_{7/2}$	$1h_{9/2}$	$1i_{13/2}$
$^{141}\text{Xe}$	$\tilde{\epsilon}_j$	3.163	2.688	2.840	1.285	1.392	0.981
	$v_j^2$	0.016	0.023	0.038	0.234	0.265	0.019
$^{143}\text{Xe}$	$\tilde{\epsilon}_j$	2.992	2.530	2.698	1.308	1.413	0.974
	$v_j^2$	0.024	0.034	0.053	0.315	0.376	0.027
$^{145}\text{Xe}$	$\tilde{\epsilon}_j$	2.814	2.366	2.546	1.328	1.454	0.966
	$v_j^2$	0.031	0.046	0.070	0.395	0.484	0.034

Third, as was done in Ref. [16], the parameters  $\Gamma_0^{sd}$  and  $\Lambda_0^{df}$  are introduced only perturbatively as they turn out to be of little importance for energy spectra. Here for simplicity a similar value to that in Ref. [16],  $\Gamma_0^{sd} = 0.15$  MeV, is employed, and  $\Lambda_0^{df} = 0$  MeV is assumed for all the odd-mass Xe nuclei under study. These values are taken to be the same for both parities in order to reduce the number of parameters.

Finally, the  $sdf$ -IBFM parameters for the  $^{145}\text{Xe}$  nucleus are determined so as to be more or less close to those determined for  $^{141,143}\text{Xe}$ , since experimental data are not available for  $^{145}\text{Xe}$ . Here it is assumed that the spin of the ground-state is  $5/2^-$ , and that the low-lying positive-parity levels exhibit a gradual decrease from  $N = 89$  to 91 as in the case of the neighboring odd-mass Ba isotopes.

The adopted strength parameters for the  $^{141,143,145}\text{Xe}$  nuclei are listed in Table III. Most of these parameters exhibit only a gradual variation with nucleon number. They are also more or less similar to those considered in the previous calculation for the odd-mass Ba nuclei [16]. An only notable difference is that the present values of the parameters  $\Gamma_0^{sd} = 0.2$  MeV and  $\Gamma_0^{ff} = 0.2$  MeV for the unique-parity configuration are much smaller than those used in Ref. [16],  $\Gamma_0^{sd} = 1.4$  MeV and  $\Gamma_0^{ff} = 1.2$  MeV.

The  $sdf$ -IBFM Hamiltonian with the parameters determined by the aforementioned procedure is numerically diagonalized [41] within the model space consisting of  $n$ ,  $s$ ,  $d$ , and  $f$  bosons and a single neutron in the full  $pfh+i_{13/2}$  shells. In the present calculation, the maximum number of  $f$  bosons,  $n_f^{\text{max}}$ , is set equal to the total number of bosons,  $n$ , that is, no restriction is made of the  $f$ -boson number, whereas in the previous study of Ref. [16] it was limited to  $n_f^{\text{max}} = 1$  in order to reduce computational time.

TABLE III. Strength parameters of the boson-fermion interaction  $\hat{V}_{\text{BF}}$  in Eq. (8) employed in the present calculation for the  $^{141,143,145}\text{Xe}$  nuclei (in MeV units). The numbers in the upper (lower) row for each nucleus correspond to the negative-parity (positive-parity) single-particle configurations.

	$\Gamma_0^{sd}$	$\Gamma_0^{ff}$	$\Lambda_0^{sd}$	$\Lambda_0^{ff}$	$A_0^d$	$A_0^f$	$\Gamma_0^{sd}$	$\Lambda_0^{df}$
$^{141}\text{Xe}$	0.20	0.20	0.0	0.0	-0.30	0.0	0.15	0.0
	0.40	0.13	0.97	0.06	-0.60	-0.15		
$^{143}\text{Xe}$	0.20	0.20	0.3	0.0	-1.5	0.0	0.15	0.0
	0.40	0.60	0.3	0.0	-0.7	-0.35		
$^{145}\text{Xe}$	0.20	0.20	0.0	0.0	0.0	0.0	0.15	0.0
	0.20	0.13	0.1	0.06	-0.4	-0.15		

In the present work electric quadrupole ( $E2$ ) and octupole ( $E3$ ) transition probabilities are analyzed. The  $E\lambda$  ( $\lambda = 2, 3$ ) operator is composed of the boson and fermion contributions:

$$\hat{T}^{(E\lambda)} = \hat{T}_{\text{B}}^{(E\lambda)} + \hat{T}_{\text{F}}^{(E\lambda)}. \quad (20)$$



For the  $E2$  operator, the bosonic part reads  $\hat{T}_B^{(E2)} = e_B^{(2)} \hat{Q}$ , with the quadrupole operator  $\hat{Q}$  defined in Eq. (4), and the fermion  $E2$  operator

$$\hat{T}_F^{(E2)} = -e_F^{(2)} \sum_{j_a j_b} \frac{1}{\sqrt{5}} \gamma_{j_a j_b}^{(2)} (a_{j_a}^\dagger \times \tilde{a}_{j_b})^{(2)}. \quad (21)$$

$e_B^{(2)}$  and  $e_F^{(2)}$  denote bosonic and fermion  $E2$  effective charges, respectively. Here  $e_B^{(2)}$  is determined for each nucleus so as to reproduce the experimental  $B(E2; 2_1^+ \rightarrow 0_1^+)$  value for the even-even Xe core [18], and the employed boson charges are  $e_B^{(2)} = 0.12$  eb (for  $^{140,141}\text{Xe}$ ), 0.158 eb (for  $^{142,143}\text{Xe}$ ), and 0.106 eb (for  $^{144,145}\text{Xe}$ ).

The fermionic effective charge  $e_F^{(2)} = 0.5$  eb is used for all the considered odd-mass Xe isotopes. Similarly, for the  $E3$  transition operator, the bosonic part reads  $\hat{T}_B^{(E3)} = e_B^{(3)} \hat{O}$ , and the fermion part can be written, in analogy to the quadrupole one, as

$$\hat{T}_F^{(E3)} = -e_F^{(3)} \sum_{j_a j_b} \frac{1}{\sqrt{7}} \gamma_{j_a j_b}^{(3)} (a_{j_a}^\dagger \times \tilde{a}_{j_b})^{(3)}. \quad (22)$$

Following Ref. [13], the  $E3$  boson effective charge  $e_B^{(3)}$  is assumed to be a function of those  $\beta_2$  and  $\beta_3$  deformations corresponding to the global minimum,  $e_B^{(3)} \propto (1 + \bar{\beta}_2 \bar{\beta}_3) \text{eb}^{3/2}$ , while the fixed  $E3$  fermion charge of  $e_F^{(3)} = 0.5 \text{eb}^{3/2}$  is employed. The adopted  $e_B^{(3)}$  values are 0.14  $\text{eb}^{3/2}$  (for  $^{140,141}\text{Xe}$ ), 0.199  $\text{eb}^{3/2}$  (for  $^{142,143}\text{Xe}$ ), and 0.14  $\text{eb}^{3/2}$  (for  $^{144,145}\text{Xe}$ ), which are determined so that the  $B(E3; 3_1^- \rightarrow 0_1^+)$  rates for the even-even nuclei are close to and exhibit similar behaviors as functions of  $N$  to those obtained in the previous *sdf*-IBM study for the neutron-rich Xe, Ba, Ce, and Nd nuclei based on the Gogny force [13].

### III. RESULTS FOR EVEN-EVEN XE

Figure 1 shows the RHB-SCMF PESs in terms of the axially symmetric quadrupole  $\beta_2$  and octupole  $\beta_3$  deformations for the even-even nuclei  $^{140,142,144}\text{Xe}$ , plotted up to the 2 MeV from the global minimum. All these nuclei exhibit prolate deformation along the  $\beta_2$  deformation with the equilibrium minimum found at  $\beta_2 \approx 0.15$ , 0.20, and 0.20 for  $^{140}\text{Xe}$ ,  $^{142}\text{Xe}$ ,  $^{144}\text{Xe}$ , respectively. Notable features are that for  $^{142}\text{Xe}$  ( $N = 88$ ) the global minimum is found at a non-zero octupole deformation,  $(\beta_2, \beta_3) = (0.2, 0.05)$ , and that the potential is soft along  $\beta_3$  deformation, as the energy at the global minimum is only 32 keV lower than the lowest energy along the  $\beta_3 = 0$  axis. These characteristics of the PESs indicate the relevance of the octupole correlations in the  $^{142}\text{Xe}$  nucleus, which also confirms that the octupole deformation is most pronounced at  $N = 88$ . In the previous study of Ref. [16], the RHB-SCMF calculation for the  $^{144}\text{Ba}$  nucleus also suggested a  $\beta_3$ -soft potential but with a much

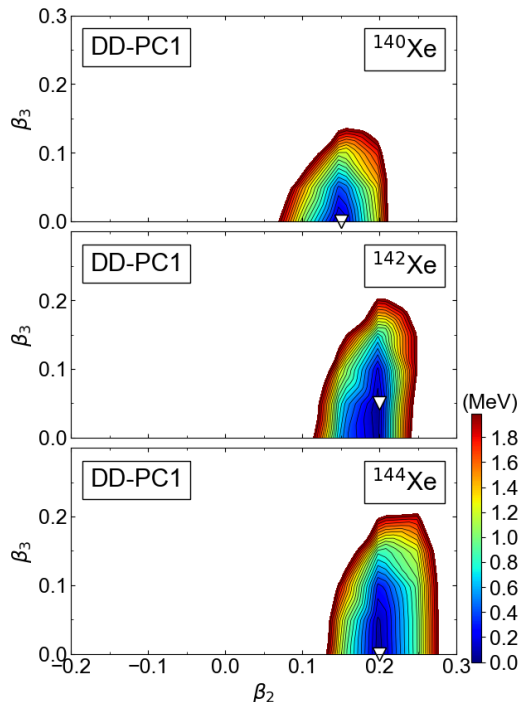


FIG. 1. Axially symmetric quadrupole ( $\beta_2$ ) - octupole ( $\beta_3$ ) constrained PESs for the even-even  $^{140,142,144}\text{Xe}$  isotopes, computed by the RHB method using the DD-PC1 functional and a separable pairing force of finite range. Total SCMF energies are plotted up to 2 MeV with respect to the global minimum, indicated by the open triangle. Energy difference between neighboring contours is 100 keV.

steeper  $\beta_3 \neq 0$  global minimum at  $(\beta_2, \beta_3) \approx (0.2, 0.1)$ . For  $^{144}\text{Xe}$ , the non-zero octupole minimum is no longer seen, but the potential is still soft in the  $\beta_3$  deformation, to a similar extent to that for the  $^{142}\text{Xe}$ .

The mapped *sdf*-IBM PESs are plotted in Fig. 2. They look rather soft particularly with respect to the  $\beta_2$  deformation as compared to the RHB-SCMF counterparts. This is a consequence of the fact that the mapping is made primarily to reproduce the topology of the RHB-SCMF PESs in the vicinity of the global minimum, specifically, the softness in the  $\beta_3$  deformation and the location of the global minimum. As for  $^{142}\text{Xe}$ , in order to see impacts of the shallow  $\beta_3 \neq 0$  minimum on energy spectra, another set of the *sdf*-IBM and *sdf*-IBFM calculations is carried out with an assumption that the minimum occurs at  $\beta_3 = 0$ , instead of  $\beta_3 = 0.05$ . The IBM PES obtained with such an assumption is also plotted in Fig. 2. The derived *sdf*-IBM parameters with the  $\beta_3 = 0$  global minimum slightly differ from those with the calculation with the non-zero octupole deformation, such that  $\epsilon_f = 0.851$  MeV and  $\chi' = -2.0$ .

Figure 3 displays the calculated low-energy positive- and negative-parity spectra for the even-even  $^{140,142,144}\text{Xe}$  isotopes, obtained from the diagonalization of the mapped *sdf*-IBM Hamiltonian (3) with

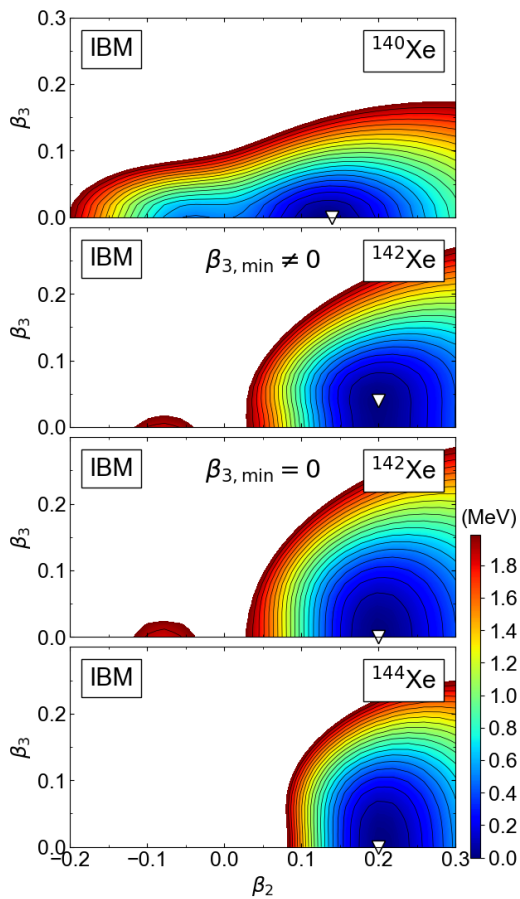


FIG. 2. Similar to the caption to Fig. 1, but for the mapped *sdf*-IBM PESs. Two different PESs for the  $^{142}\text{Xe}$  are obtained by taking  $\beta_3 = 0.05$  ( $\neq 0$ ) as the global minimum consistent with the corresponding RHB-SCMF PES in Fig. 1, and by assuming that the global minimum occurs at  $\beta_3 = 0$ .

parameters determined from the RHB-SCMF calculations. The results are compared with the experimental data available at ENSDF database of NNDC [18]. The calculation reasonably reproduces the  $2_1^+$  energies, but the energy levels in the ground-state bands are rather overestimated for higher-spin states with  $I^\pi > 4^+$ . This is partly due to the limited number of bosons considered in the *sdf*-IBM, i.e.,  $n = 4, 5$ , and  $6$  for  $^{140,142,144}\text{Xe}$ , respectively, which may be insufficient to account for the energies for the states higher than  $I^\pi = 4^+$ . For all the even-even Xe nuclei, the *sdf*-IBM predicts the lowest negative-parity state to be  $I^\pi = 3^-$ , above which the  $1^-$  level appears. In the previous study of Ref. [16] a similar level structure of negative-parity odd-spin states to those of  $^{140,142,144}\text{Xe}$ , shown in Fig. 3, were obtained for  $^{142}\text{Ba}$ , where octupole deformation is minor. For  $^{144,146}\text{Ba}$ , on the other hand, the *sdf*-IBM predicted a rather rotational-like negative-parity yrast band, with the bandhead being the  $1^-$  state [16]. For  $^{140}\text{Xe}$  the present *sdf*-IBM calculation reproduces the  $3^-$  energy

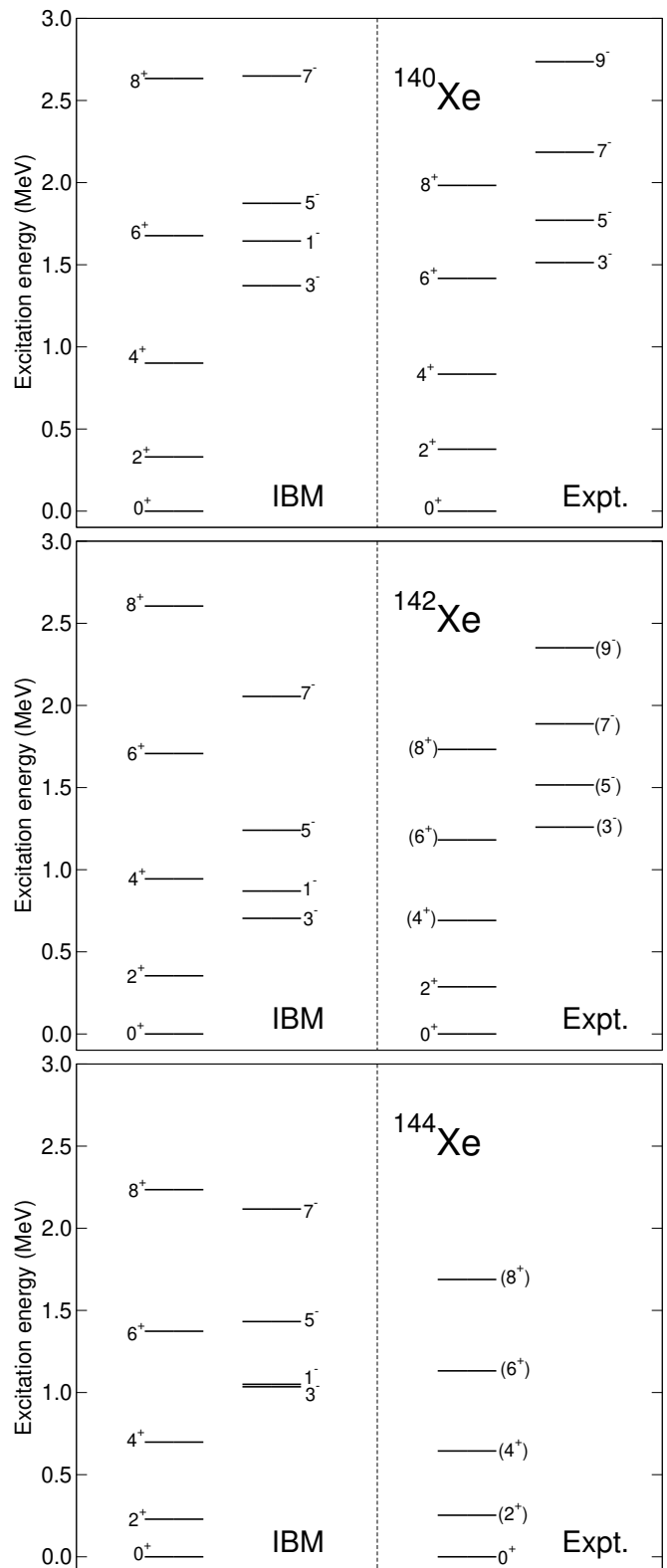


FIG. 3. Calculated low-energy positive- and negative-parity spectra for the even-even  $^{140,142,144}\text{Xe}$  nuclei. Experimental data are taken from the ENSDF database [18].

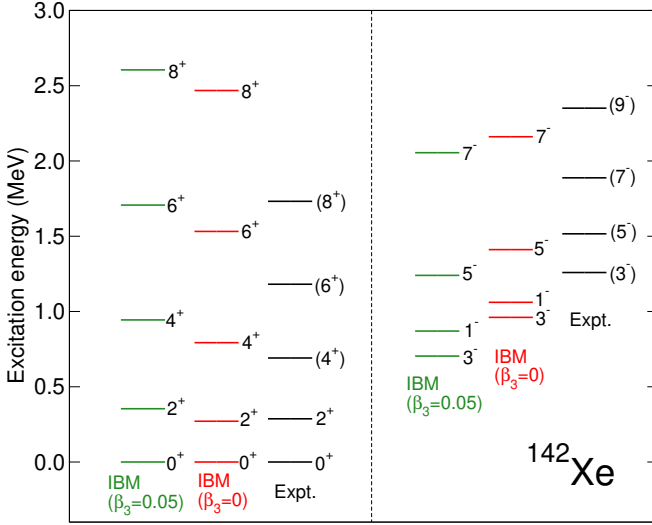


FIG. 4. Same as Fig. 3, but for the calculated energy spectra for the  $^{142}\text{Xe}$  nucleus obtained by taking the  $\beta_3 = 0.05 (\neq 0)$  global minimum and by assuming that the minimum occurs at  $\beta_3 = 0$ .

reasonably well, while the higher-spin negative-parity levels are overestimated. For  $^{142}\text{Xe}$ , the mapped *sdf*-IBM gives much lower  $3^-$  and  $5^-$  energy levels than the experimental values, which reflects the pronounced  $\beta_3$  softness with  $\beta_3 \neq 0$  global minimum in its PES (see Fig. 1).

Figure 4 compares between the *sdf*-IBM energy spectra obtained with and without taking into account the non-zero octupole minimum in the mapping procedure. A notable difference between the two *sdf*-IBM results is that the negative-parity levels obtained with the  $\beta_3 = 0$  minimum are higher in energy than those obtained with  $\beta_3 \neq 0$ , and this difference indicates that the octupole effects taken into account in the *sdf*-IBM are less significant in the former calculation than in the latter.

In Table IV expectation values of the *f*-boson number operator  $\langle \hat{n}_f \rangle$  calculated for the positive- and negative-parity yrast states are presented. For  $^{140}\text{Xe}$ , *f* bosons appear to play a minor role in the positive-parity states, since the expectation value  $\langle \hat{n}_f \rangle < 0.1$ , whereas the negative-parity states are described by one-*f*-boson configurations. In  $^{142}\text{Xe}$ , the *f*-boson contributions are suggested to be significant even in the ground state,  $\langle \hat{n}_f \rangle > 1$ . This finding is similar to that of the previous mapped *sdf*-IBM calculation for the neutron-rich even-even Xe nuclei based on the Gogny EDF [13]. Table IV shows that large amounts of the *f*-boson components are present also in the calculated states for  $^{144}\text{Xe}$ .

Table V lists predicted  $B(E2)$  and  $B(E3)$  transition rates for the low-spin positive- and negative-parity states of the even-even  $^{140,142,144}\text{Xe}$  nuclei, in comparison with the experimental data [18]. There is no experimental data available for  $^{142,144}\text{Xe}$ , other than the  $B(E2; 2_1^+ \rightarrow$

$0_1^+$ ) rates [18]. The present mapped *sdf*-IBM calculation predicts in-band  $E2$  transitions within the ground-state band. The predicted  $B(E2; 5_1^- \rightarrow 3_1^-)$  transition probability for  $^{140}\text{Xe}$  underestimates the experimental value. The calculation suggests sizable  $E3$  transitions of  $B(E3; 3_1^- \rightarrow 0_1^+) \approx 20 - 30$  Weisskopf units (W.u.) for the studied even-even Xe isotopes.

TABLE IV. Expectation values of the *f*-boson number operator  $\langle \hat{n}_f \rangle$  for the yrast states for  $^{140,142,144}\text{Xe}$ .

$I^\pi$	$^{140}\text{Xe}$	$^{142}\text{Xe}$	$^{144}\text{Xe}$
$0_1^+$	0.058	1.121	0.575
$2_1^+$	0.031	0.818	0.467
$4_1^+$	0.014	0.585	0.353
$6_1^+$	0.005	0.772	0.253
$8_1^+$	0.001	1.508	0.172
$1_1^-$	1.019	1.434	1.366
$3_1^-$	1.046	1.714	1.460
$5_1^-$	1.017	1.432	1.344
$7_1^-$	1.004	1.241	1.229

TABLE V.  $B(E2)$  and  $B(E3)$  transition rates in Weisskopf units (W.u.) for the low-lying states of the even-even  $^{140,142,144}\text{Xe}$  nuclei calculated with the mapped *sdf*-IBM, and the experimental data available at the NNDC [18].

A	$B(E\lambda; I_i^\pi \rightarrow I_f^\pi)$	<i>sdf</i> -IBM (W.u.)	Expt. (W.u.)
$^{140}\text{Xe}$	$B(E2; 2_1^+ \rightarrow 0_1^+)$	24.1	$24.0 \pm 0.7$
	$B(E2; 4_1^+ \rightarrow 2_1^+)$	32.5	$45_{-6}^{+9}$
	$B(E2; 6_1^+ \rightarrow 4_1^+)$	28.6	$> 22.6$
	$B(E2; 5_1^- \rightarrow 3_1^-)$	16.5	$64_{-22}^{+38}$
	$B(E3; 3_1^- \rightarrow 0_1^+)$	34.7	
	$B(E3; 5_1^- \rightarrow 2_1^+)$	41.0	
	$B(E3; 7_1^- \rightarrow 4_1^+)$	34.0	
$^{142}\text{Xe}$	$B(E2; 2_1^+ \rightarrow 0_1^+)$	31.4	$31.4 \pm 4.5$
	$B(E2; 4_1^+ \rightarrow 2_1^+)$	52.5	
	$B(E2; 6_1^+ \rightarrow 4_1^+)$	48.0	
	$B(E3; 3_1^- \rightarrow 0_1^+)$	21.5	
	$B(E3; 5_1^- \rightarrow 2_1^+)$	40.7	
$^{144}\text{Xe}$	$B(E3; 7_1^- \rightarrow 4_1^+)$	53.3	
	$B(E2; 2_1^+ \rightarrow 0_1^+)$	32.6	$32.6 \pm 7.6$
	$B(E2; 4_1^+ \rightarrow 2_1^+)$	46.7	
	$B(E2; 6_1^+ \rightarrow 4_1^+)$	48.6	
	$B(E3; 3_1^- \rightarrow 0_1^+)$	20.9	
	$B(E3; 5_1^- \rightarrow 2_1^+)$	33.7	
	$B(E3; 7_1^- \rightarrow 4_1^+)$	39.6	

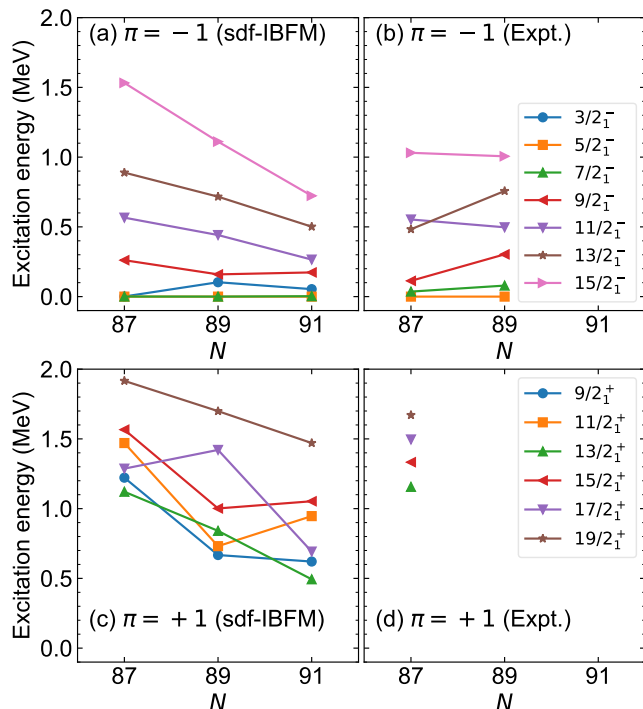


FIG. 5. Evolution of low-lying negative-parity [ $\pi = -1$ , (a) and (b)] and positive-parity [ $\pi = +1$ , (c) and (d)] spectra for the odd-mass nuclei  $^{141,143,145}\text{Xe}$  as functions of  $N$ . The calculated results from the *sdf*-IBFM are shown in (a) and (c), and the experimental data [18] are depicted in (b) and (d).

## IV. RESULTS FOR ODD-MASS XE

### A. Evolution of energy levels

In Fig. 5 calculated low-lying positive- and negative-parity energy spectra for the odd-mass  $^{141,143,145}\text{Xe}$  nuclei are depicted as functions of  $N$ , obtained from the *sdf*-IBFM with a microscopic input provided by the RHB-SCMF calculation using the DD-PC1 EDF. Experimental spectra adopted from the NNDC [18] are also plotted. The present calculation suggests that the negative-parity states are composed mainly of the configurations of a single neutron in the normal-parity (*pfh*) orbitals coupled to the *sd*-boson space. The decreasing pattern of the calculated negative-parity levels reflects evolution of the quadrupole collectivity with increasing valence nucleon number. The behaviors of the calculated  $9/2_1^-$  and  $13/2_1^-$  levels from  $N = 87$  to 89 are, however, at variance with the experimental ones which rather increase with  $N$ . A reasonable agreement with the observed negative-parity levels is obtained for  $^{143}\text{Xe}$ .

In Fig. 5(c), one can observe that the structure of the calculated positive-parity levels for  $^{143}\text{Xe}$  is rather different from those of the adjacent nuclei  $^{141,145}\text{Xe}$ , namely, at  $N = 89$  the  $9/2_1^+$  and  $11/2_1^+$  levels become particu-

larly low in energy such that they are below the  $13/2_1^+$  level. The change in the nuclear structure at  $N = 89$  correlates with the fact that for  $^{142}\text{Xe}$  a potential is rather soft and exhibits a non-zero  $\beta_3$  minimum. Such a feature of the PES is supposed to be reflected in some of those derived *sdf*-IBM parameters for  $^{142}\text{Xe}$  that are relevant to the octupole degree of freedom, and hence in the fitted boson-fermion interaction strengths for  $^{143}\text{Xe}$ . For example, as shown in Table I the single-*f* boson energy  $\epsilon_f$  is rather low at  $^{142}\text{Xe}$  as compared to those derived for  $^{140,144}\text{Xe}$ , and the largest value of the parameter  $\chi'$  is chosen for  $^{142}\text{Xe}$  among the three even-even Xe nuclei. Also in Table III the parameter  $\Lambda_0^{ff} = 0.60$  MeV, employed for the positive-parity states of  $^{143}\text{Xe}$ , is much larger than the corresponding values for  $^{141,145}\text{Xe}$ . As will be shown, many of the low-energy positive-parity states for  $^{143}\text{Xe}$  are accounted for by large amounts of octupole-boson contributions, whereas in  $^{141}\text{Xe}$  the dominant configurations in these positive-parity states are based on the neutron  $\nu 1i_{13/2}$  single-particle orbital coupled to the *sd*-boson space.

### B. Detailed energy spectrum

Figures 6–9 depict detailed energy spectra resulting from the *sdf*-IBFM calculations. The calculated energy levels shown in Figs. 6, 7, and 9 are grouped into bands so as to follow dominant  $\Delta I = 2$  *E2* transitions between states and the increasing order of the angular momenta. The experimental data are taken from the NNDC [18].

#### 1. $^{141}\text{Xe}$

The even-even core nucleus  $^{140}\text{Xe}$  is here suggested to be mostly quadrupole deformed, and hence the octupole effects are also expected to be weak in the odd-mass neighbor  $^{141}\text{Xe}$ . In the experimental studies of Refs. [19, 20] two pairs of  $\Delta I = 2$  bands, one consisting of the  $5/2_1^-$  and  $15/2_1^+$  bands, and the other of the  $11/2_1^-$  and  $13/2_1^+$  bands were interpreted as simplex symmetry partners with  $s = \mp i$ , respectively. As shown in Fig. 6 negative-parity bands built on the  $3/2_1^+$ ,  $5/2_1^+$ ,  $7/2_1^+$ , and  $9/2_1^+$  states are suggested by the *sdf*-IBFM. These bands are connected by only weak *E2* transitions, which are typically less than 10 W.u., and are uniformly stretched in energy in comparison to the observed ones.

The present calculation, however, gives the  $\Delta I = 2$  positive-parity band built on the  $13/2_1^+$  level, with the band-head level in agreement with experiment. The predicted  $13/2_1^+$  band also exhibits large *E2* transitions:  $B(E2; 17/2_1^+ \rightarrow 13/2_1^+) = 39$  W.u., and  $B(E2; 21/2_1^+ \rightarrow 17/2_1^+) = 38$  W.u. Experimentally a  $\Delta I = 2$  band built on the  $15/2_1^+$  level at 1333 keV is observed. At about the same excitation energy a band that starts from the  $11/2_1^+$  state is obtained within the *sdf*-IBFM, which



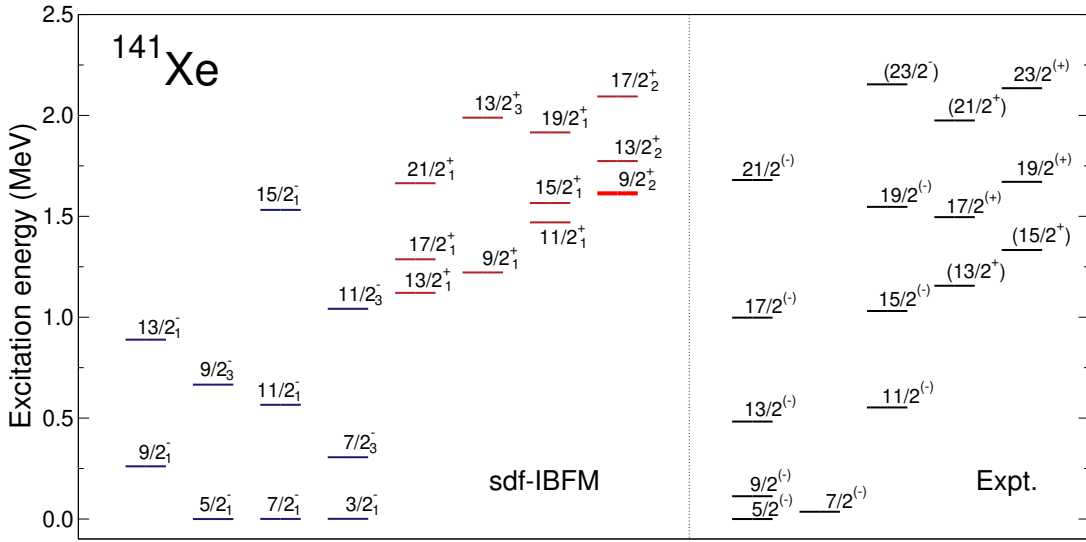


FIG. 6. Calculated and experimental [18] low-energy spectra for  $^{141}\text{Xe}$ . Those calculated states that contain more than one  $f$ -bosons in the wave functions,  $\langle \hat{n}_f \rangle > 1$ , are highlighted in thick lines.

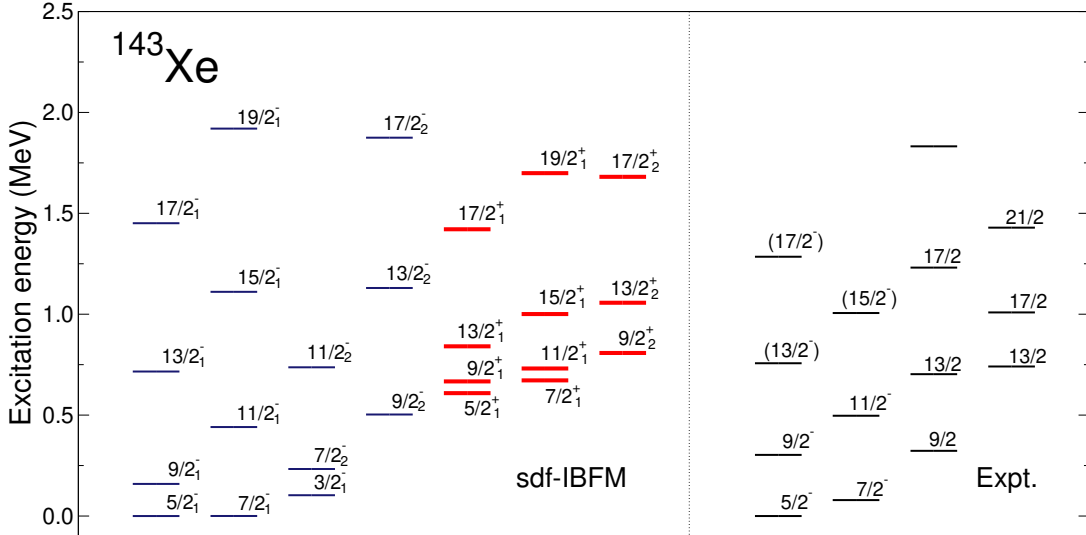


FIG. 7. Same as Fig. 6, but for  $^{143}\text{Xe}$ . Experimental data are taken from Ref. [21].

is connected by the  $E2$  transitions of  $B(E2; 15/2_1^+ \rightarrow 11/2_1^+) = 27$  W.u., and  $B(E2; 19/2_1^+ \rightarrow 15/2_1^+) = 30$  W.u.

As in Table IV, Table VI gives expectation values of the  $f$ -boson  $\hat{n}_f$  [Eq. (3)] and single-neutron  $\hat{n}_j$  number operators calculated by using the *sdf*-IBFM wave functions. It is suggested that the low-lying negative-parity states are made mainly of the normal-parity ( $\nu 2f_{7/2}$  and  $\nu 1h_{9/2}$ ) configurations, while there is practically no contribution from  $f$  bosons. The positive-parity states are predominantly made of the  $\nu 1i_{13/2}$  configuration, i.e.,  $\langle \hat{n}_{13/2} \rangle \approx 1$ , whereas the octupole contributions are negligible, except for the  $9/2_2^+$  state.

## 2. $^{143}\text{Xe}$

As shown in Sec. III the RHB-SCMF result suggests a non-zero octupole minimum on the  $(\beta_2, \beta_3)$ -PES for the even-even nucleus  $^{142}\text{Xe}$ , and hence the octupole correlations are supposed to be most pronounced in  $^{143}\text{Xe}$  among the considered odd-mass Xe nuclei. The proposed level scheme for  $^{143}\text{Xe}$  is depicted in Fig. 7, and the structures of the *sdf*-IBFM wave functions of the calculated states are shown in Table VII. The experimental data are taken from Ref. [21], suggesting the low-lying negative-parity  $\Delta I = 2$  bands built on the  $5/2_1^-$  and  $7/2_1^-$  states which are lying close in energy to each other. The present

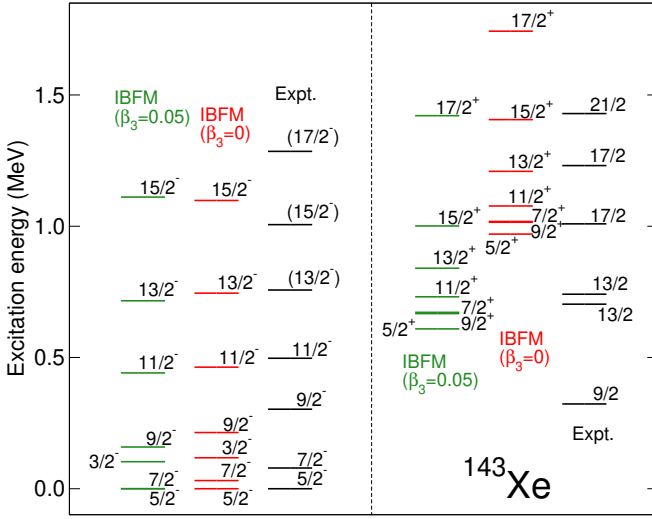


FIG. 8. Calculated negative- (left) and positive-parity (right) energy spectra for the  $^{143}\text{Xe}$  nucleus obtained with the non-zero octupole ( $\beta_3 = 0.05 \neq 0$ ) global minimum and with the assumption of the zero-octupole ( $\beta_3 = 0$ ) minimum in the mapping. Experimental data are taken from Ref. [21]. Note that the parity of the experimental levels shown on the right-hand side has not been determined.

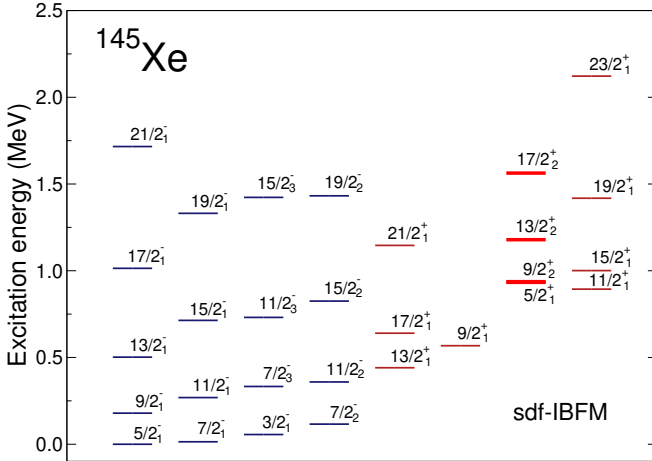


FIG. 9. Calculated low-energy spectra for  $^{145}\text{Xe}$ .

*sdf*-IBFM reproduces these observed bands reasonably well. The  $9/2_1^-$  level is here underestimated, probably due to a strong level repulsion between the first and second  $9/2^-$  states. The calculation predicts additional bands built on the  $9/2_2^-$  state at  $E_x = 0.503$  MeV, and on the  $3/2_1^-$  state lying close to the  $5/2_1^-$  ground state. Experimental data from Ref. [21] suggest two bands based on the states with spins 9/2 and 13/2, but with parity undetermined.

Table VII shows that there are sizable amounts of the *f*-boson components in the negative-parity states, i.e., the expectation value  $\langle \hat{n}_f \rangle \approx 0.5$ . The *f*-boson ef-

TABLE VI. Expectation values of the *f*-boson number operator  $\hat{n}_f$ , and the single-particle operators  $\hat{n}_j$  corresponding to each orbital in those states for the  $^{141}\text{Xe}$  nucleus shown in Fig. 6.

$I^\pi$	$\langle \hat{n}_f \rangle$	$\langle n_j \rangle$					
		$3p_{1/2}$	$3p_{3/2}$	$2f_{5/2}$	$2f_{7/2}$	$1h_{9/2}$	$1i_{13/2}$
$3/2_1^-$	0.012	0.006	0.039	0.018	0.657	0.279	0.002
$5/2_1^-$	0.009	0.006	0.001	0.046	0.030	0.916	0.000
$7/2_1^-$	0.008	0.002	0.007	0.020	0.248	0.722	0.000
$7/2_3^-$	0.015	0.004	0.014	0.024	0.377	0.581	0.001
$9/2_1^-$	0.003	0.006	0.014	0.021	0.344	0.615	0.000
$9/2_2^-$	0.002	0.011	0.014	0.022	0.385	0.567	0.000
$11/2_1^-$	0.001	0.008	0.015	0.022	0.413	0.543	0.000
$11/2_3^-$	0.005	0.006	0.008	0.018	0.381	0.588	0.000
$13/2_1^-$	0.000	0.015	0.026	0.019	0.412	0.527	0.000
$13/2_3^-$	0.001	0.000	0.035	0.080	0.520	0.364	0.000
$15/2_1^-$	0.001	0.000	0.050	0.063	0.310	0.576	0.000
$9/2_1^+$	0.033	0.000	0.000	0.000	0.013	0.001	0.985
$9/2_2^+$	1.003	0.003	0.005	0.022	0.134	0.833	0.004
$11/2_1^+$	0.040	0.000	0.000	0.000	0.018	0.003	0.978
$13/2_1^+$	0.033	0.000	0.000	0.000	0.004	0.000	0.996
$13/2_2^+$	0.038	0.000	0.000	0.000	0.014	0.002	0.984
$15/2_1^+$	0.023	0.000	0.000	0.000	0.004	0.000	0.996
$17/2_1^+$	0.021	0.000	0.000	0.000	0.002	0.000	0.998
$17/2_2^+$	0.015	0.000	0.000	0.000	0.004	0.000	0.996
$19/2_1^+$	0.011	0.000	0.000	0.000	0.001	0.000	0.998
$21/2_1^+$	0.010	0.000	0.000	0.000	0.001	0.000	0.999

fects are suggested to be even more pronounced in the positive-parity states, i.e.,  $\langle \hat{n}_f \rangle \approx 1.5$ . In the present *sdf*-IBFM calculation, the positive-parity bands based on the  $5/2_1^+$ ,  $7/2_1^+$ , and  $9/2_2^+$  band heads are suggested to be of octupole nature (highlighted as thick lines in Fig. 7), since in the wave functions of those states belonging to these bands significant amounts of the *f*-boson components are present, with the expectation values typically  $\langle \hat{n}_f \rangle \approx 1.4 - 1.7$  (see Table VII).

Figure 8 compares the *sdf*-IBFM energy spectra calculated with and without taking into account the  $\beta_3 \neq 0$  global minimum in the mapping procedure for the even-even core  $^{142}\text{Xe}$ . The same boson-fermion strength parameters are used for the two different *sdf*-IBFM calculations, the only difference being in the Hamiltonian parameters for the even-even core. It is suggested that the negative-parity states are not affected by the assumption of the zero octupole minimum in the mapping, since the negative-parity states are mainly comprised of normal-parity single-particle configurations coupled to the *sd*-boson space, whereas the *f*-boson contributions are minor,  $\langle \hat{n}_f \rangle \approx 0.5$  [cf. Table VII]. On the other hand, the positive-parity levels calculated with the  $\beta_3 = 0$  minimum are higher than those with the  $\beta_3 \neq 0$  minimum, since the positive-parity states for  $^{143}\text{Xe}$  are mostly of octupole nature, i.e.,  $\langle \hat{n}_f \rangle \approx 1.5$ , and are affected by the presence of the  $\beta_3 \neq 0$  minimum.

TABLE VII. Similar to the caption to Table VI, but for  $^{143}\text{Xe}$ .

$I^\pi$	$\langle \hat{n}_f \rangle$	$\langle n_j \rangle$					
		$3p_{1/2}$	$3p_{3/2}$	$2f_{5/2}$	$2f_{7/2}$	$1h_{9/2}$	$1i_{13/2}$
$3/2_1^-$	0.615	0.023	0.123	0.013	0.565	0.276	0.000
$5/2_1^-$	0.527	0.001	0.006	0.056	0.055	0.882	0.000
$7/2_1^-$	0.643	0.000	0.003	0.019	0.060	0.917	0.000
$7/2_2^-$	0.553	0.008	0.060	0.018	0.264	0.650	0.000
$9/2_1^-$	0.790	0.001	0.001	0.032	0.043	0.923	0.000
$9/2_2^-$	0.423	0.001	0.013	0.022	0.138	0.826	0.000
$11/2_1^-$	0.624	0.000	0.004	0.015	0.059	0.921	0.000
$11/2_2^-$	0.663	0.022	0.158	0.013	0.484	0.323	0.000
$13/2_1^-$	0.697	0.004	0.001	0.051	0.037	0.907	0.000
$13/2_2^-$	0.408	0.001	0.011	0.023	0.121	0.844	0.000
$15/2_1^-$	0.512	0.000	0.007	0.012	0.075	0.907	0.000
$17/2_1^-$	0.627	0.009	0.001	0.087	0.031	0.871	0.000
$17/2_2^-$	0.711	0.004	0.006	0.062	0.089	0.839	0.000
$19/2_1^-$	0.728	0.000	0.010	0.010	0.086	0.894	0.000
$5/2_1^+$	1.492	0.004	0.006	0.051	0.036	0.902	0.000
$7/2_1^+$	1.477	0.051	0.037	0.084	0.065	0.763	0.000
$9/2_1^+$	1.445	0.003	0.009	0.046	0.057	0.884	0.000
$9/2_2^+$	1.671	0.060	0.317	0.021	0.468	0.134	0.000
$11/2_1^+$	1.429	0.009	0.010	0.031	0.048	0.902	0.000
$13/2_1^+$	1.550	0.002	0.006	0.029	0.048	0.914	0.000
$13/2_2^+$	1.735	0.015	0.182	0.013	0.717	0.075	0.000
$15/2_1^+$	1.712	0.001	0.001	0.031	0.018	0.949	0.000
$17/2_1^+$	1.401	0.001	0.007	0.016	0.061	0.915	0.000
$17/2_2^+$	1.499	0.011	0.184	0.017	0.707	0.080	0.000
$19/2_1^+$	1.502	0.001	0.000	0.049	0.011	0.939	0.000

3.  $^{145}\text{Xe}$ 

The RHB-SCMF calculation for the even-even core nucleus  $^{144}\text{Xe}$  suggests a  $\beta_3$ -soft potential in the SCMF calculation, so the octupole correlations are still expected to play non-negligible roles in the neighboring  $^{145}\text{Xe}$ . Figure 9 exhibits the predicted level scheme for  $^{145}\text{Xe}$ , and the wave function contents of the relevant states are shown in Table VIII. Note that experimental information is currently not available for  $^{145}\text{Xe}$ . Figure 9 displays four negative-parity  $\Delta I = 2$  bands connected by strong  $E2$  transitions. As one sees in Table VIII, negative-parity states are mostly composed of the  $\nu 2f_{7/2}$  and  $\nu 1h_{9/2}$  normal-parity configurations coupled to the  $sd$ -boson space, whereas contributions from  $f$  bosons are present but not significant, since as the expectation values within the range  $\langle \hat{n}_f \rangle \approx 0.2 - 0.4$ .

From Table VIII, for the positive-parity yrast states of  $^{145}\text{Xe}$ , such as the  $9/2_1^+$ ,  $11/2_1^+$  and  $13/2_1^+$  states, the contributions from the  $\nu 1i_{13/2}$  single-neutron configurations play much more important roles in many of the positive-parity states than in  $^{143}\text{Xe}$ , while the  $f$  boson contents are relatively small,  $\langle \hat{n}_f \rangle \approx 0.4 - 0.5$ . The  $sd$ -IBFM produces the low-lying positive-parity  $13/2_1^+$  and

TABLE VIII. Similar to the caption to Table VI, but for  $^{145}\text{Xe}$ .

$I^\pi$	$\langle \hat{n}_f \rangle$	$\langle n_j \rangle$					
		$3p_{1/2}$	$3p_{3/2}$	$2f_{5/2}$	$2f_{7/2}$	$1h_{9/2}$	$1i_{13/2}$
$3/2_1^-$	0.425	0.004	0.111	0.001	0.836	0.045	0.002
$5/2_1^-$	0.402	0.000	0.019	0.004	0.947	0.028	0.002
$7/2_1^-$	0.491	0.001	0.050	0.002	0.915	0.030	0.002
$7/2_2^-$	0.400	0.000	0.001	0.009	0.152	0.837	0.000
$7/2_3^-$	0.386	0.004	0.088	0.003	0.838	0.066	0.002
$9/2_1^-$	0.445	0.000	0.004	0.008	0.136	0.851	0.000
$9/2_2^-$	0.411	0.000	0.012	0.007	0.861	0.117	0.002
$11/2_1^-$	0.433	0.001	0.048	0.001	0.814	0.134	0.002
$11/2_2^-$	0.410	0.000	0.004	0.011	0.154	0.831	0.000
$13/2_1^-$	0.408	0.000	0.002	0.013	0.053	0.932	0.000
$13/2_2^-$	0.328	0.000	0.012	0.006	0.919	0.059	0.004
$15/2_1^-$	0.341	0.000	0.039	0.000	0.706	0.252	0.003
$17/2_1^-$	0.331	0.000	0.001	0.018	0.034	0.947	0.000
$17/2_2^-$	0.245	0.000	0.009	0.006	0.939	0.039	0.007
$19/2_1^-$	0.268	0.000	0.030	0.000	0.640	0.311	0.018
$5/2_1^+$	1.404	0.023	0.134	0.013	0.760	0.035	0.034
$9/2_1^+$	0.431	0.000	0.000	0.000	0.002	0.000	0.998
$9/2_2^+$	1.381	0.002	0.081	0.002	0.902	0.008	0.005
$11/2_1^+$	0.441	0.000	0.000	0.000	0.008	0.000	0.992
$13/2_1^+$	0.516	0.000	0.000	0.000	0.002	0.000	0.997
$13/2_2^+$	1.423	0.000	0.046	0.002	0.925	0.007	0.020
$15/2_1^+$	0.444	0.000	0.000	0.000	0.006	0.001	0.994
$17/2_1^+$	0.432	0.000	0.000	0.000	0.003	0.000	0.997
$17/2_2^+$	1.318	0.000	0.035	0.001	0.905	0.025	0.033
$19/2_1^+$	0.350	0.000	0.000	0.000	0.006	0.001	0.993
$21/2_1^+$	0.324	0.000	0.000	0.000	0.002	0.000	0.997
$23/2_1^+$	0.255	0.000	0.000	0.000	0.005	0.001	0.993

$11/2_1^+$  bands, with the bandheads being at  $E_x \approx 0.493$  MeV and 0.946 MeV, respectively. These bands are mainly made of the  $sd$ -boson coupled mainly to the  $\nu 1h_{9/2}$  single-particle orbital (see Table VIII). The  $f$ -boson components make significant contributions to determine the wave functions of the non-yrast positive-parity states,  $\langle \hat{n}_f \rangle \approx 1.3 - 1.4$ . The  $5/2_1^+$  level at 933 keV is primarily of octupole nature,  $\langle \hat{n}_f \rangle \approx 1.4$ , similarly to  $^{143}\text{Xe}$ . The band built on this state, shown in thick lines in Fig. 9, is of octupole nature as it turns out to be  $\langle \hat{n}_f \rangle \approx 1.3 - 1.4$  for the corresponding  $sd$ -IBFM wave functions.

## C. Transition properties

Table IX shows the calculated  $B(E2)$  and  $B(E3)$  transition strengths for yrast states of the odd-mass  $^{141,143,145}\text{Xe}$  nuclei. The calculated  $B(E2)$  rates for  $^{143,145}\text{Xe}$  are generally larger than those for  $^{141}\text{Xe}$ , reflecting that the quadrupole collectivity increases from  $^{141}\text{Xe}$  to  $^{143,145}\text{Xe}$  isotopes. Some transition rates, such as the  $B(E2; 9/2_1^- \rightarrow 5/2_1^-)$ , and  $B(E2; 11/2_1^+ \rightarrow 7/2_1^+)$

ones are predicted to be large in  $^{143}\text{Xe}$ , while they are much more smaller in  $^{141,145}\text{Xe}$ , suggesting that the nuclear structure of  $^{143}\text{Xe}$  differs from the adjacent nuclei  $^{141,145}\text{Xe}$ . For all the three nuclei, large  $\Delta I = 2$  in-band  $E2$  transition rates for the positive-parity states,  $B(E2; 13/2_1^+ \rightarrow 9/2_1^+)$ ,  $B(E2; 15/2_1^+ \rightarrow 11/2_1^+)$ ,  $B(E2; 17/2_1^+ \rightarrow 13/2_1^+)$ , and  $B(E2; 19/2_1^+ \rightarrow 15/2_1^+)$ , are obtained. The  $B(E3)$  rates predicted for  $^{143}\text{Xe}$  are generally large, as compared to  $^{141,145}\text{Xe}$ , which are also considered to be a signature of octupole correlations in  $^{143}\text{Xe}$ .

## V. CONCLUSIONS

To summarize, signatures of octupole correlations in the neutron-rich odd-mass Xe isotopes near  $N = 88$  have been studied within the theoretical framework of the nuclear EDF and *sdf*-IBFM. The *sdf*-IBM Hamiltonian describing quadrupole and octupole collective states of the even-even nuclei, and single-particle energies and occupation probabilities of an unpaired neutron, were determined by using the results of the RHB-SCMF calculations based on the relativistic EDF. Strength parameters for the boson-fermion interactions were, however, empirically determined so as to reproduce the observed low-lying levels in each odd-mass Xe nucleus, and energy-level systematic in the neighboring odd-mass Ba nuclei.

The microscopic RHB-SCMF calculations suggested

TABLE IX. Predicted  $B(E2)$  and  $B(E3)$  transition rates (in W.u.) for the low-lying states of the odd-mass  $^{141,143,145}\text{Xe}$  nuclei, calculated with the *sdf*-IBFM.

$B(E\lambda; I_i^\pi \rightarrow I_f^\pi)$	$^{141}\text{Xe}$	$^{143}\text{Xe}$	$^{145}\text{Xe}$
$B(E2; 3/2_1^- \rightarrow 5/2_1^-)$	1.3	19.7	30.96
$B(E2; 3/2_1^- \rightarrow 7/2_1^-)$	0.5	5.9	54.61
$B(E2; 7/2_1^- \rightarrow 5/2_1^-)$	0.2	48.5	43.25
$B(E2; 9/2_1^- \rightarrow 5/2_1^-)$	0.1	22.8	6.02
$B(E2; 11/2_1^- \rightarrow 7/2_1^-)$	6.1	39.2	47.85
$B(E2; 13/2_1^- \rightarrow 9/2_1^-)$	7.8	61.9	38.77
$B(E2; 15/2_1^- \rightarrow 11/2_1^-)$	2.7	68.9	57.19
$B(E2; 17/2_1^- \rightarrow 13/2_1^-)$	0.6	77.2	51.58
$B(E2; 9/2_1^+ \rightarrow 5/2_1^+)$	23.0	18.2	1.59
$B(E2; 11/2_1^+ \rightarrow 7/2_1^+)$	5.6	25.1	0.68
$B(E2; 13/2_1^+ \rightarrow 9/2_1^+)$	34.9	45.2	54.01
$B(E2; 15/2_1^+ \rightarrow 11/2_1^+)$	26.6	42.9	42.74
$B(E2; 17/2_1^+ \rightarrow 13/2_1^+)$	39.0	56.9	59.97
$B(E2; 19/2_1^+ \rightarrow 15/2_1^+)$	30.4	64.5	50.79
$B(E2; 21/2_1^+ \rightarrow 17/2_1^+)$	37.7	61.6	61.78
$B(E3; 9/2_1^+ \rightarrow 3/2_1^-)$	2.9	2.2	5.54
$B(E3; 11/2_1^+ \rightarrow 5/2_1^-)$	0.2	14.0	4.64
$B(E3; 13/2_1^+ \rightarrow 7/2_1^-)$	0.0	18.5	8.95
$B(E3; 15/2_1^+ \rightarrow 9/2_1^-)$	0.0	23.3	0.78
$B(E3; 17/2_1^+ \rightarrow 11/2_1^-)$	0.0	33.3	9.23

for  $^{142}\text{Xe}$  a potential that is notably soft along the octupole  $\beta_3$  deformation with a shallow, but non-zero octupole global mean-field minimum at  $\beta_3 \approx 0.05$ . There is no octupole deformed minimum in  $^{140}\text{Xe}$  and  $^{144}\text{Xe}$ , while in the latter nucleus the potential was shown to be quite soft in the  $\beta_3$  direction and hence the octupole degree of freedom should not be negligible. The calculated energy spectra for the even-even Xe nuclei showed certain traces of the octupole correlations, including the low-energy negative-parity states of octupole nature at  $^{142}\text{Xe}$ . The octupole degree of freedom has been shown to have influences on the low-lying spectra for the neighboring odd-mass Xe nuclei. The evolution of the low-energy spectra as functions of  $N$  and their wave function contents suggested a variation of nuclear structure in the vicinity of  $N = 88$ , at which octupole collectivity is expected to be most pronounced. In particular, many of the low-lying positive-parity states for  $^{143}\text{Xe}$  were shown to contain more than one  $f$  bosons in their wave functions, and to exhibit sizable amounts of the  $E3$  transitions to the negative-parity ground-state band.

The present work has suggested that the octupole correlations still play a part in describing those states of the odd-mass Xe isotopes with the excitation energies  $E_x \gtrsim 0.5$  MeV, similarly to the neighboring odd-mass Ba isotopes. The results of the present spectroscopic calculations would stimulate experimental studies aimed to access those neutron-rich Xe isotopes that are far from the  $N = 82$  shell closure, which also have been beyond reach of microscopic nuclear structure calculations. Possible future studies include an application of the *sdf*-IBFM to more challenging cases of light actinides, for which static octupole deformation is suggested. On the other hand, since the boson-fermion strength parameters were here obtained using only limited experimental information and based on the assumption that the low-lying structures of the odd-mass Xe nuclei should be similar to those of the neighboring Ba nuclei, the reliability of these parameters remains an open question. It can be addressed, ideally, by developing a method to determine all of the boson-fermion interaction strengths in a fully microscopic way, that is, only by using results of the EDF-SCMF calculation and without referring to the experimental data. The works along these lines are in progress and will be reported elsewhere.

## ACKNOWLEDGMENTS

The author thanks Atsuko Odahara and Kenichi Yoshida for valuable discussions. This work has been supported in part by the RCNP Collaboration Research Network program as the Project No. COREnet-051.



- [1] P. A. Butler and W. Nazarewicz, *Rev. Mod. Phys.* **68**, 349 (1996).
- [2] J. Engel, M. J. Ramsey-Musolf, and U. van Kolck, *Prog. Part. and Nucl. Phys.* **71**, 21 (2013).
- [3] L. P. Gaffney, P. A. Butler, M. Scheck, A. B. Hayes, F. Wenander, M. Albers, B. Bastin, C. Bauer, A. Blazhev, S. Bönig, N. Bree, J. Cederkäll, T. Chupp, D. Cline, T. E. Cocolios, T. Davinson, H. D. Witte, J. Diriken, T. Grahn, A. Herzan, M. Huyse, D. G. Jenkins, D. T. Joss, N. Kesteloot, J. Konki, M. Kowalczyk, T. Kröll, E. Kwan, R. Lutter, K. Moschner, P. Napiorkowski, J. Pakarinen, M. Pfeiffer, D. Radeck, P. Reiter, K. Reynders, S. V. Rigby, L. M. Robledo, M. Rudigier, S. Sambi, M. Seidlitz, B. Siebeck, T. Stora, P. Thoele, P. V. Duppen, M. J. Vermeulen, M. von Schmid, D. Voulot, N. Warr, K. Wimmer, K. Wrzosek-Lipska, C. Y. Wu, and M. Zielinska, *Nature (London)* **497**, 199 (2013).
- [4] B. Bucher, S. Zhu, C. Y. Wu, R. V. F. Janssens, D. Cline, A. B. Hayes, M. Albers, A. D. Ayangeakaa, P. A. Butler, C. M. Campbell, M. P. Carpenter, C. J. Chiara, J. A. Clark, H. L. Crawford, M. Cromaz, H. M. David, C. Dickerson, E. T. Gregor, J. Harker, C. R. Hoffman, B. P. Kay, F. G. Kondev, A. Korichi, T. Lauritsen, A. O. Macchiavelli, R. C. Pardo, A. Richard, M. A. Riley, G. Savard, M. Scheck, D. Seweryniak, M. K. Smith, R. Vondrasek, and A. Wiens, *Phys. Rev. Lett.* **116**, 112503 (2016).
- [5] B. Bucher, S. Zhu, C. Y. Wu, R. V. F. Janssens, R. N. Bernard, L. M. Robledo, T. R. Rodríguez, D. Cline, A. B. Hayes, A. D. Ayangeakaa, M. Q. Buckner, C. M. Campbell, M. P. Carpenter, J. A. Clark, H. L. Crawford, H. M. David, C. Dickerson, J. Harker, C. R. Hoffman, B. P. Kay, F. G. Kondev, T. Lauritsen, A. O. Macchiavelli, R. C. Pardo, G. Savard, D. Seweryniak, and R. Vondrasek, *Phys. Rev. Lett.* **118**, 152504 (2017).
- [6] A. Yagi, A. Odahara, H. Nishibata, R. Lozeva, C.-B. Moon, S. Nishimura, K. Yoshida, N. Yoshinaga, C. Watanabe, K. Higashiyama, T. Shimoda, R. Daido, Y. Fang, P. S. Lee, B. Moon, P. Doornenbal, G. Lorusso, P.-A. Söderström, T. Sumikama, H. Watanabe, T. Isobe, H. Baba, H. Sakurai, F. Browne, Z. Patel, S. Rice, L. Sinclair, J. Wu, Z. Y. Xu, R. Yokoyama, T. Kubo, N. Inabe, H. Suzuki, N. Fukuda, D. Kameda, H. Takeda, D. S. Ahn, Y. Shimizu, D. Murai, F. L. Bello Garrote, J.-M. Daugas, F. Didierjean, E. Ideguchi, S. Iimura, T. Ishigaki, H. S. Jung, T. Komatsubara, Y. K. Kwon, C. S. Lee, S. Morimoto, M. Niikura, I. Nishizuka, and K. Tshoo, *Phys. Rev. C* **105**, 044325 (2022).
- [7] Nurhafiza M. Nor, *Nuclear structures in neutron-rich nuclei  $^{141}\text{Xe}$  and  $^{143}\text{Xe}$  investigated by  $\beta - \gamma$  spectroscopy*, Doctoral Thesis, Osaka University (2024).
- [8] Nurhafiza M. Nor *et al.*, to be submitted.
- [9] F. Iachello and P. Van Isacker, *The interacting boson-fermion model* (Cambridge University Press, Cambridge, 1991).
- [10] K. Nomura, D. Vretenar, and B.-N. Lu, *Phys. Rev. C* **88**, 021303 (2013).
- [11] K. Nomura, D. Vretenar, T. Nikšić, and B.-N. Lu, *Phys. Rev. C* **89**, 024312 (2014).
- [12] K. Nomura, *Int. J. Mod. Phys. E* **32**, 2340001 (2023), <https://doi.org/10.1142/S0218301323400013>.
- [13] K. Nomura, R. Rodríguez-Guzmán, L. M. Robledo, J. E. García-Ramos, and N. C. Hernández, *Phys. Rev. C* **104**, 044324 (2021).
- [14] K. Nomura, *Phys. Rev. C* **105**, 054318 (2022).
- [15] K. Nomura, *Phys. Rev. C* **106**, 024330 (2022).
- [16] K. Nomura, T. Nikšić, and D. Vretenar, *Phys. Rev. C* **97**, 024317 (2018).
- [17] T. Rzaca-Urban, W. Urban, J. A. Pinston, G. S. Simpson, A. G. Smith, and I. Ahmad, *Phys. Rev. C* **86**, 044324 (2012).
- [18] Brookhaven National Nuclear Data Center, <http://www.nndc.bnl.gov>.
- [19] W. Urban, N. Schulz, M. Bentaleb, E. Lubkiewicz, J. L. Durell, M. J. Leddy, M. A. Jones, W. R. Phillips, A. G. Smith, B. J. Varley, I. Ahmad, and L. R. Morss, *Eur. Phys. J. A* **8**, 5 (2000).
- [20] Y. Huang, S. J. Zhu, J. H. Hamilton, Y. J. Chen, E. H. Wang, A. V. Ramayya, Z. G. Xiao, H. J. Li, Y. X. Luo, J. O. Rasmussen, G. M. Ter-Akopian, and Y. T. Oganessian, *Journal of Physics G: Nuclear and Particle Physics* **44**, 095101 (2017).
- [21] T. Rzaca-Urban, W. Urban, J. A. Pinston, A. G. Smith, and I. Ahmad, *Phys. Rev. C* **83**, 067301 (2011).
- [22] D. Vretenar, A. V. Afanasjev, G. A. Lalazissis, and P. Ring, *Phys. Rep.* **409**, 101 (2005).
- [23] T. Nikšić, D. Vretenar, and P. Ring, *Prog. Part. Nucl. Phys.* **66**, 519 (2011).
- [24] T. Nikšić, D. Vretenar, and P. Ring, *Phys. Rev. C* **78**, 034318 (2008).
- [25] Y. Tian, Z. Y. Ma, and P. Ring, *Phys. Lett. B* **676**, 44 (2009).
- [26] J. Engel and F. Iachello, *Phys. Rev. Lett.* **54**, 1126 (1985).
- [27] A. F. Barfield, B. R. Barrett, J. L. Wood, and O. Scholten, *Ann. Phys.* **182**, 344 (1988).
- [28] F. Iachello and A. Arima, *The interacting boson model* (Cambridge University Press, Cambridge, 1987).
- [29] T. Otsuka, A. Arima, F. Iachello, and I. Talmi, *Phys. Lett. B* **76**, 139 (1978).
- [30] T. Otsuka, A. Arima, and F. Iachello, *Nucl. Phys. A* **309**, 1 (1978).
- [31] J. N. Ginocchio and M. W. Kirson, *Nucl. Phys. A* **350**, 31 (1980).
- [32] A. Bohr and B. R. Mottelson, *Nuclear Structure*, Vol. II (Benjamin, New York, USA, 1975).
- [33] K. Nomura, N. Shimizu, and T. Otsuka, *Phys. Rev. Lett.* **101**, 142501 (2008).
- [34] K. Nomura, N. Shimizu, and T. Otsuka, *Phys. Rev. C* **81**, 044307 (2010).
- [35] H. Schaaser and D. Brink, *Nucl. Phys. A* **452**, 1 (1986).
- [36] D. R. Inglis, *Phys. Rev.* **103**, 1786 (1956).
- [37] S. Beliaev, *Nucl. Phys.* **24**, 322 (1961).
- [38] K. Nomura, T. Otsuka, N. Shimizu, and L. Guo, *Phys. Rev. C* **83**, 041302 (2011).
- [39] O. Scholten, *Prog. Part. Nucl. Phys.* **14**, 189 (1985).
- [40] K. Nomura, T. Nikšić, and D. Vretenar, *Phys. Rev. C* **93**, 054305 (2016).
- [41] S. Heinze, computer program ARBMODEL, University of Cologne (2008).